Int. J. Electron. Commun. (AEÜ) 164 (2023) 154624

Contents lists available at ScienceDirect

International Journal of Electronics and Communications

journal homepage: www.elsevier.com/locate/aeue

Regular paper

Design of a modified hairpin bandpass filter using embedded radial stubs featuring ultrawide stopband

Mohammad Sharifi [a], Valiollah Mashayekhi [b,*]

[a] Department of Electrical Engineering, Amirkabir University of Technology, Tehran, Iran
[b] Department of Electrical Engineering, Shahrood University of Technology, Shahrood, Iran

ARTICLE INFO

Keywords:
Bandpass filter
Hairpin
Harmonic suppression
Spurious suppression
Wide stopband

ABSTRACT

The analysis and design of a microstrip bandpass filter featuring an ultrawide stopband are presented and investigated in this paper. In this filter, single radial stubs are exploited in combination with a regular hairpin structure to achieve suppression of harmonic responses of the filter passband up to $10f_0$. The passband of the filter remains almost intact compared to the conventional hairpin filter. A 3rd-order BPF with a central frequency of 2 GHz and a bandwidth of 44% is designed and the simulation results are verified with the measurement results. The proposed filter shows more than 32 dB rejection from 3 GHz to 20 GHz in S21 and the measured passband insertion loss is 1.3 dB. The filter structure is simple, without the need for defected ground structures, multilayers, lumped elements, and even vias. The proposed filter can be in demand anywhere easy fabrication, low cost, ultrawide stopband together with a good rejection level are considered crucial.

1. Introduction

Bandpass filters are extensively used in many RF and microwave systems to select the desired bandwidth and remove interfering signals from the environment or circuit elements [1]. Moreover, the constant increase in the RF frequency range in use has led to the emergence of signal transmitters in the previously vacant bands, intensifying the necessity for filters with wider stopbands for RF front-ends in the receivers. On the other hand, output spectral purity requirement in transmitters and synthesizers has become stricter in a similar manner justifying the need for filters with wide stopbands [2]. In addition to these, even within an RF system, there are circuit chains containing non-linear elements, such as amplifiers and multipliers that produce unwanted signals exactly at the harmonics of the desired passband which should be suppressed before finding their way into other parts of the system and causing problems by themselves or their mixed products [3–6].

Among different bandpass filter technologies including waveguide, coaxial, dielectric resonator, and microstrip [7], microstrip filters are quite popular due to their low cost, small size, low profile, and ease of fabrication and integration [8] and [9]. End-coupled bandpass filters were among the earliest introduced microstrip bandpass filters [10]. Edge-coupled bandpass filters [11], based on half-wavelength resonators, have half of the size of the end-coupled filters and are one of the most popular bandpass microstrip filters. Hairpin filters [12] can be considered the folded version of the edge-coupled filters occupying smaller spaces. However, both filters suffer from poor stopband response due to spurious harmonics at the multiples of the passband central frequency (nf_0 ($n = 2, 3, \ldots$, f_0 is the central frequency of the passband).

Numerous various methods have been proposed to improve the stopband rejection of a microstrip bandpass filter. One simple method is to cascade an additional low-pass filter to the existing bandpass filter which will increase the total insertion loss. Over-coupled end stages may be used to suppress the second harmonic [13]. Slots in the ground plane and substrate suspension of a filter can be used to eliminate the spurious response [14,15]. Split ring resonators (SRR), cross-coupling, meandered miniaturized structures, and also meandered shaped coupled lines may be used to reject the spurious response [16–19]. Different fractional techniques can also be used to suppress the spurious harmonics [20–22]. Periodically nonuniform coupled microstrip lines may be applied for the unwanted band suppression [23]. Using multilayers and stepped resonance resonators (SIR) can improve the upper stopband by eliminating the second and third harmonics [24,25]. Cutting grooves in the filter substrate can also suppress the second harmonic [26]. T-shaped spurlines and trapezoidal- shaped meander spurlines have also been used to improve the stopband in folded hairpin bandpass filters [27,28]. These techniques only address the rejection of up to the third harmonic

* Corresponding author.
E-mail address: vmashayekhi@shahroodut.ac.ir (V. Mashayekhi).

https://doi.org/10.1016/j.aeue.2023.154624
Received 31 December 2022; Accepted 10 March 2023
Available online 16 March 2023

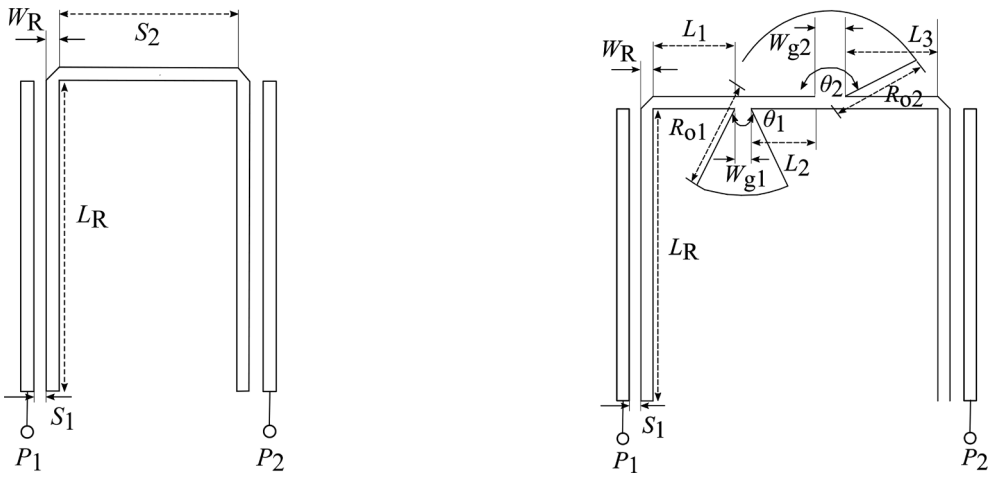

Fig. 1. (a) Traditional hairpin resonator, (b) Proposed hairpin resonator.

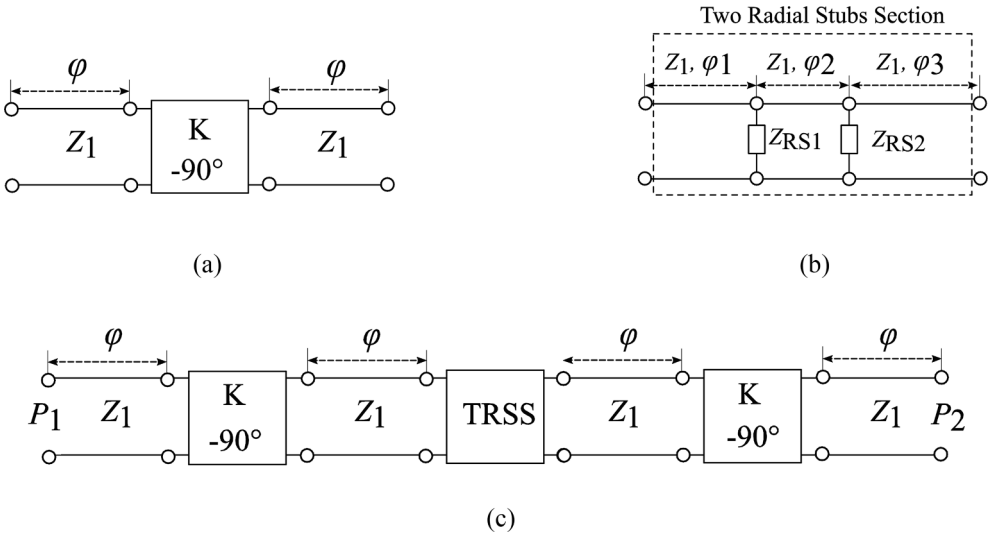

Fig. 2. Equivalent circuits of (a) Coupled lines. (b) Two consecutive radial stubs and connecting transmission lines. (c) The proposed resonator.

response of the filter. There also have been some efforts to widen the stopband beyond the third harmonic. Sinusoidal variations on the width of the coupled lines, shortened coupled sections, loaded stepped impedance resonators, and stub-loaded resonators can be used to extend the rejection band beyond the third harmonic [29–34]. The aforementioned designs have disadvantages including the increased difficulty of fabrication due to factors such as etching in the substrate or structures in the ground plane, which elevates the cost and the complexity of development or having relatively many small sections and design parameters which increases the optimization time and also makes filters sensitive to production tolerances. Additionally, many of the filters are focused only on suppressing the first few harmonics.

In this paper, a modified hairpin bandpass filter is introduced to suppress spurious responses of the regular hairpin microstrip filter. The conventional hairpin filter bandwidth is almost intact in this design. This filter does not require any defected ground structure (DGS), substrate etching, lumped elements, or vias which can be of interest from an industrial point of view. The filter does not include many sections and is more production tolerance resilient. Considering the fabrication ease and its high performance, this filter can be used in industrial mass production projects where every little saving counts. Based on the proposed design, a 3rd-order filter is designed with a central frequency of 2 GHz. Using radial stubs embedded in the resonators, a stopband of up to $10f_0$ (20 GHz) with a rejection of more than 32 dB is achieved. The paper structure is as follows. In Section 2, the filter design is described. In Section 3, a detailed examination of radial stubs is presented. The experimental verification of the design simulations is shown in Section 4. Finally, this paper is concluded in Section 5.

2. Filter design

The layout of a traditional hairpin resonator and the proposed resonator is shown in Fig. 1. The structure of the suggested resonator can be divided into six sections: input coupled lines (ICL), line 1 (L1), radial stub 1 (RS1), line 2 (L2), radial stub 2 (RS2), line 3 (L3), and output coupled lines (OCL). The effect of miters is neglected in the design. The whole resonator can be treated as a cascading network of individual elements. The equivalent circuits for the coupled lines and the section of two radial stubs are shown in Fig. 2(a) and (b) where Z_1 and φ represent the impedance and the electrical length of the coupled lines and Z_{RS1}, Z_{RS2}, Z_1, φ_1, φ_2, φ_3 represent the impedances of radial stub 1, radial stub 2, connecting transmission lines, and the electrical lengths of line 1, line 2, and line 3, respectively. The two radial stubs section (TRSS) consists of two consecutive radial stubs with connecting transmission lines, and the total cascading network of the proposed resonator is shown in Fig. 2 (c). The circuit is assumed to be lossless for analysis. The total circuit

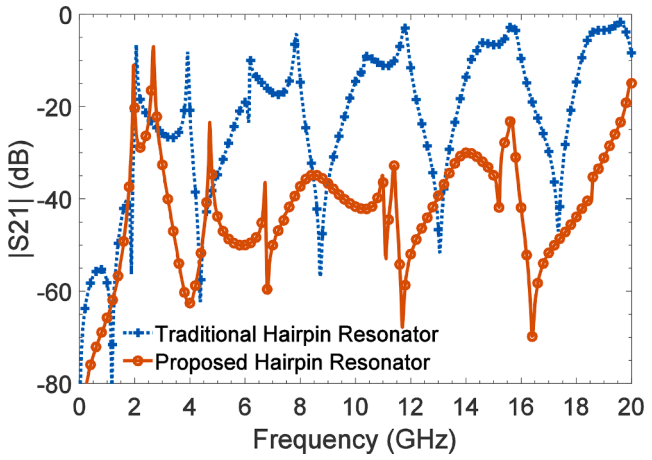

Fig. 3. Frequency response of the traditional hairpin resonator and the proposed resonator. Dimensions: Traditional: $L_R = 23$ mm, $W_R = 0.2$ mm, $S_1 = 1$ mm, $S_2 = 1$ mm. Proposed: $L_R = 17$ mm, $W_R = 0.2$ mm, $S_1 = 1$ mm, $L_1 = 4.2$ mm, $L_2 = 4$ m, $L_3 = 4.2$ mm, $R_{O1} = 5.1$ mm, $W_{g1} = 1$ mm, $\theta_1 = 126°$, $R_{O2} = 2.6$ mm, $W_{g2} = 0.6$ mm. $\theta_2 = 91°$.

network of Fig. 2(c) can be derived from the cascaded transmission matrices of different elements which is equal to Eq. (1):

$$[T_{Total}] = [T_{ICL}][T_{L1}][T_{RS1}][T_{L2}][T_{RS2}][T_{L3}][T_{OCL}] \tag{1}$$

The transmission matrix of the input or output coupled lines is given by Eq. (2) [35],

$$[T_{ICL/OCL}] = \begin{bmatrix} \left(JZ_1 + \frac{1}{JZ_1}\right)sin\theta cos\theta & j\left(JZ_1^2 sin^2\theta - \frac{cos^2\theta}{J}\right) \\ j\left(\frac{1}{JZ_1^2}sin^2\theta - Jcos^2\theta\right) & \left(JZ_1 + \frac{1}{JZ_1}\right)sin\theta cos\theta \end{bmatrix} \tag{2}$$

For lossless transmission lines before, in the middle, and after the radial stubs, the transfer matrix is given by Eq. (3) [36],

$$[T_{L_i}] = \begin{pmatrix} cos\beta l_i & jZ_1 sin\beta l_i \\ jY_1 sin\beta l_i & cos\beta l_i \end{pmatrix}_{i=1,2,3} \tag{3}$$

In addition, the input impedance of the radial stubs can be expressed as Eq. (4) [37]

$$Z_{RS_1/RS_2} = -\frac{j120\pi h}{R_i\theta\sqrt{\varepsilon_{eff}}}\frac{N_0(\beta R_i)J_1(\beta R_o) - J_0(\beta R_i)N_1(\beta R_o)}{J_1(\beta R_i)N_1(\beta R_o) - N_1(\beta R_i)J_1(\beta R_o)} \tag{4}$$

where J_m is the Bessel function of the first kind and N_m is the Neumann function (Bessel function of the second kind) of order m, $\beta = 2\pi(\varepsilon_{eff})^{1/2}/\lambda_0$ is the phase constant, h is the dielectric layer thickness, and ε_{eff} is the effective dielectric constant calculated for an equivalent microstrip line with a width of $w = (R_o + R_i)\sin(\theta/2)$. For providing simplicity and consistency with simulation software, the R_i parameter of radial stubs is replaced by W_g which is described by Eq. (5).

$$W_g = 2R_i tan\left(\frac{\theta}{2}\right). \tag{5}$$

From the relationships between scattering and transmission matrices [35], the total response of the modified hairpin resonator can be obtained using Eqs. (1)–(4).

The comparison of frequency responses of traditional and proposed hairpin resonator are shown in Fig. 3. The substrate used for the simulations is Rogers RO4003c with a relative dielectric constant or $\varepsilon_r = 3.55$, dielectric loss tangent of 0.0027, and thickness of 0.508 mm. The operation frequency of both resonators is 2 GHz. For the regular resonator, the periodic emergence of spurious spikes at the harmonics of the resonant frequency narrows the rejection band. Whereas the proposed

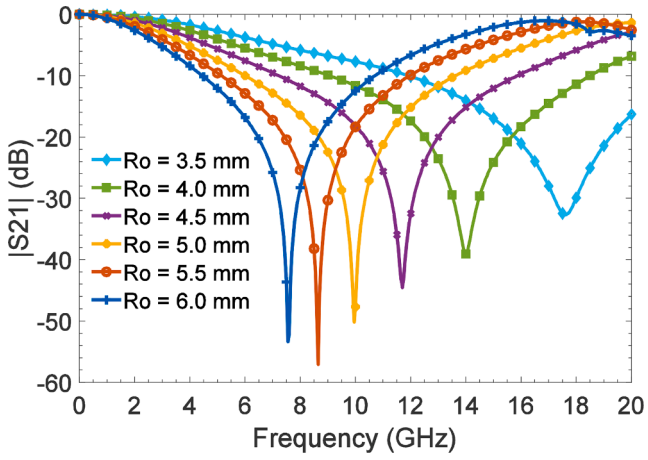

(a)

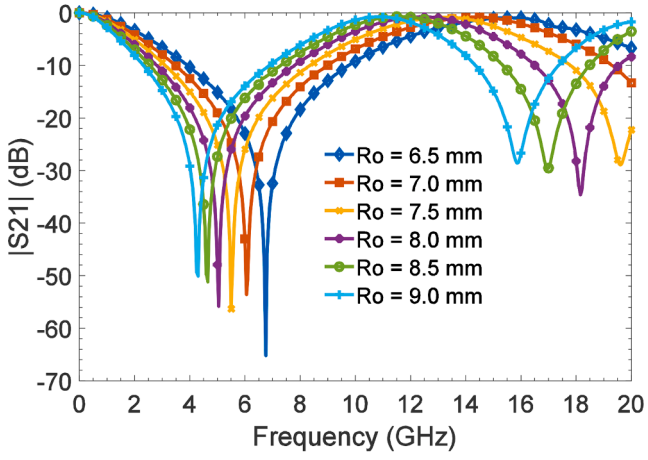

(b)

Fig. 4. Single radial stub frequency response with regard to R_O sweep. (a) Ro sweep from 3.5 mm to 6 mm. (b) R_O sweep from 6.5 mm to 9 mm. Other values are: $\theta = 50°$, $W_g = 1$ mm, $W_R = 0.2$ mm.

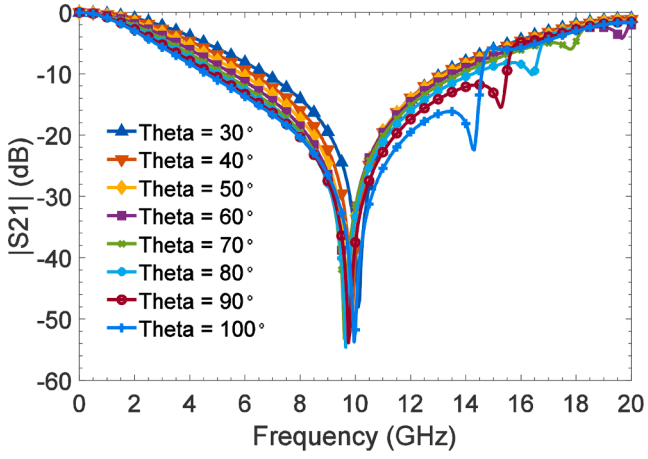

Fig. 5. Single radial stub frequency response with regard to θ sweep. Other values are: $R_O = 5$, $W_g = 1$ mm, $W_R = 0.2$ mm.

resonator presents not only a very broad stopband, it also introduces a significant stopband rejection. Changing different parameters of the radial stubs affects the stopband range and suppression level which is

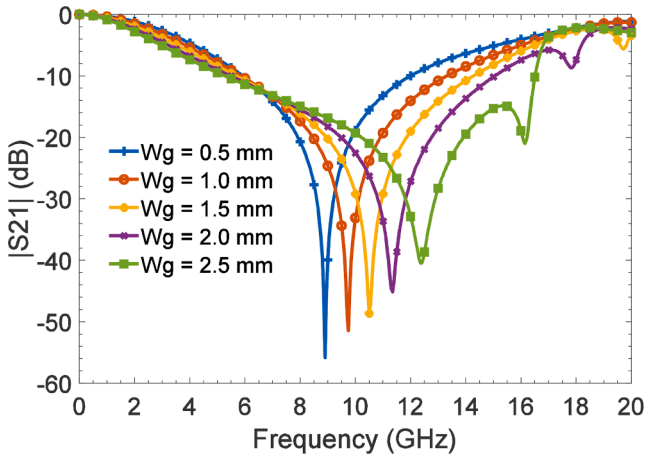

Fig. 6. Single radial stub frequency response with regard to W_g sweep. Other values are: $R_O = 5$, $\theta = 50°$, $W_R = 0.2$ mm.

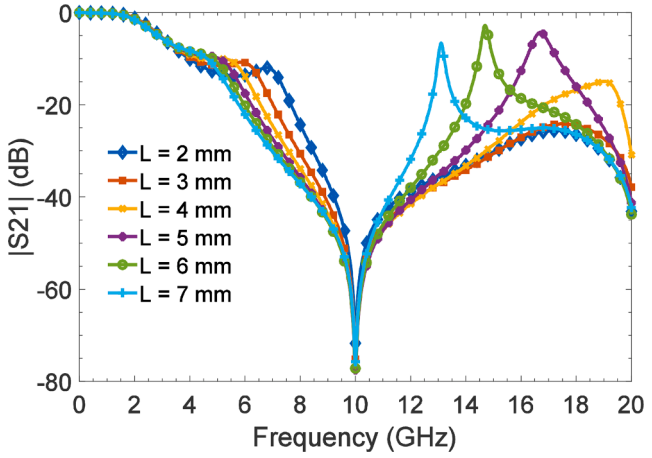

Fig. 7. Frequency response of two consecutive radial stub with regard to the sweep of the length of connecting transmission line between them. Other values are: $W_R = 0.2$ mm, $S_1 = 1$ mm, $L_1 = 5$ mm, $L_3 = 5$ mm, $R_{O1} = 5.1$ mm, $W_{g1} = 1$ mm, $\theta_1 = 126°$, $R_{O2} = 2.6$ mm, $W_{g2} = 0.6$ mm. $\theta_2 = 91°$.

investigated in the following section.

3. Radial stubs

In general, a single radial stub acts as a low pass element and when connected to coupled lines can suppress spurious responses. The effects of changing different parameters of a radial stub which is designed to have a cutoff frequency larger than 2 GHz are shown in Figs. 4-6. The variation of R_o has a significant effect on the cutoff frequency and as is clear from Fig. 4, by increasing the $R_{o,}$ the cutoff frequency reduces which is foreseeable because with moving to lower frequencies the dimensions of a microwave element increase. The change in theta almost does not lead to a change in the radius, so as expected it does not affect the cutoff frequency significantly but changes the slopes of the frequency response which is illustrated in Fig. 5. Finally, from Fig. 6, we can see that the change in W_g also effects the cutoff frequency. This is expected as an increase in W_g while keeping the angle constant can be considered as moving the radial stub more towards the line which will lead to a decrease in the realized radius of the radial stub and therefore moving the notch in S21 to higher frequencies.

Although the suppression band of a radial stub is wide, it ultimately rises and deteriorates the frequency response by the appearance of its spurious response, which can be seen in Fig. 4(a) and (b). To overcome this problem and provide an ultrawide rejection band, two consecutive radials are embedded in every resonator. Therefore, the rise in the response of larger radial stubs whose cutoff frequencies is located in lower frequencies can get compensated by the frequency responses of the smaller radial stubs with higher cutoff frequencies.

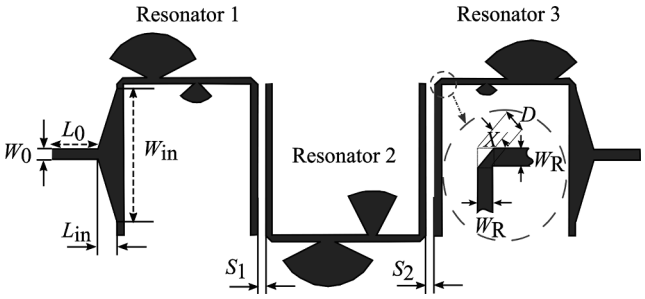

Fig. 8. Schematic of the proposed filter design.

The combination of two radial stubs and connected transmission lines acts as a more sophisticated low pass section and provides wider rejection with deeper suppression. The input and output connected transmission lines of the TRSS do not affect the frequency response radically and only change the slope of the frequency response to some extent. However, the effect of the middle connecting line is significant and can cause the rise of a spurious response. The frequency response of a TRSS with parameter sweep of the middle line is shown in Fig. 7. The two stubs are positioned in an alternating manner, this decreases the possibility of unwanted couplings between radial stubs which is important from some viewpoints. These unwanted couplings are not modeled in the equivalent circuit analysis of the proposed resonator and increase the complexity of the design without any obvious advantages. Moreover, these couplings cannot be modeled in the circuit-based simulator of AWR, which is used for the early stages of optimization of the filter, and therefore will lead to a larger discrepancy between responses in the circuit-based and the full-wave simulations. Alternating the stubs also allows the length of connecting the transmission line between the two stubs to be shorter. The smaller stub is usually placed inside the resonator to decrease the unwanted coupling between the coupled lines and the radial stubs as much as possible.

4. Simulated and experimental results

The design procedure for the proposed filter architecture is described in the following:

1) Designing the coupled lines according to the central frequency of the bandpass filter.
2) Designing the radial stubs according to Eq. (4) with a cutoff frequency greater than the passband upper limit to provide a coverage of the desired stopband by uniform distribution of the radial stubs notches. In this way, radial stubs would cover the rise of the spurious response of each other up to the upper limit of the stopband.
3) Performing optimization procedure for the proposed filter with available microstrip elements in AWR software using the calculated values in previous section.
4) Optimizing the filter in the full-wave simulation software HFSS with the obtained values from AWR software as the initial values for the design process.
5) Further optimization in HFSS is performed to compensate the uncounted limitations of the circuit-based software, such as limited accuracy of the element models, nonmodeled proximity couplings, and etc., to obtain the required return loss in the passband and the suppression bandwidth along with the rejection level.

A 3rd-order filter with central frequency of 2 GHz is considered and

Table 1
Dimensions of the designed BPF.

Resonator 1	R_{o1}	θ_1	W_{g1}	R_{o2}	θ_2	W_{g2}	L_1	L_2	L_3	
	5.21	103.4°	5.28	1.24	108.7°	0.6	1.56	2.04	4.77	
Resonator 2	R_{o1}	θ_2	W_{g1}	R_{o2}	θ_2	W_{g2}	L_1	L_2	L_3	
	3.59	110.7°	0.3	7.07	51.3°	0.7	6.37	2.6	6.47	
Resonator 3	R_{o1}	θ_1	W_{g1}	R_{o2}	θ_2	W_{g2}	L_1	L_2	L_3	
	5.13	125.7°	1	2.6	91.2°	0.57	5.81	4.04	2.82	
Others	W_0	L_0	W_{in}	L_{in}	L_R	W_R	S_1	S_2	D	X
	1.13	5.18	7.44	2.1	17.5	0.2	0.2	0.2	0.14	0.14

Note: The unit for length is mm.

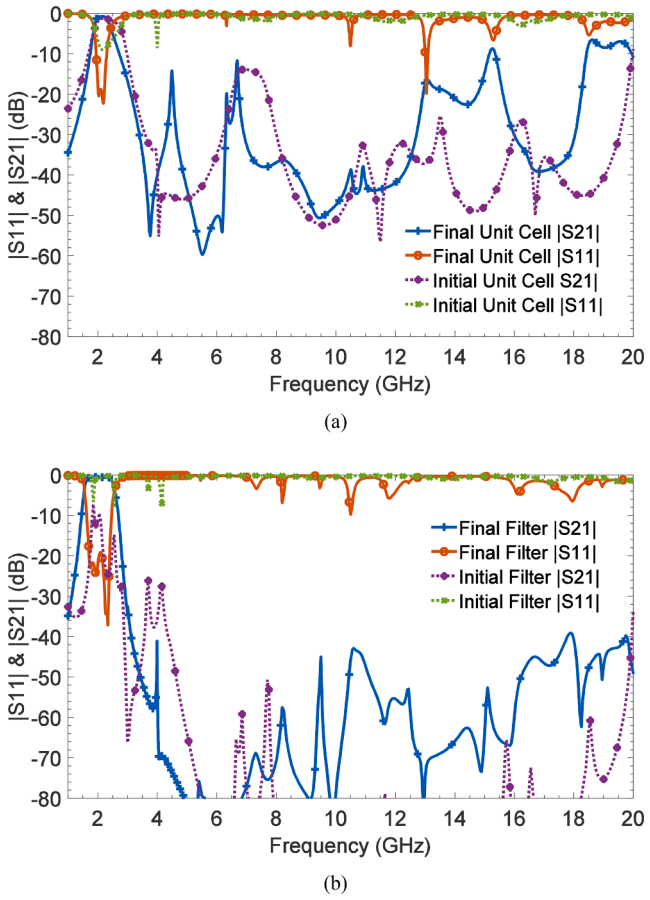

Fig. 9. Simulated frequency responses of the filter with the initial design parameters and the final full-wave simulation for: (a) A single unit of the filter. (b) The complete filter.

designed using the proposed resonator. The Rogers RO4003c is used as the substrate which is a regular and accessible substrate. It has a relative dielectric constant of $\varepsilon_r = 3.55$, a dielectric loss tangent of 0.0027, and a thickness of 0.508 mm. The schematic of the proposed structure is presented in Fig. 8 and the parameter values are given in Table 1. The size of the filter, excluding the 50-ohm input and output traces, is 5.1 cm × 3.4 cm which is equal to $0.64\lambda g \times 0.43\lambda g$.

The comparison of the frequency responses of the initial and final optimized design of the proposed structure are presented in Fig. 9. The former is obtained using AWR circuit-based simulator and the initial design values for the equivalent circuit in Fig. 2(c) and the latter is obtained using the full-wave simulation in HFSS. The comparisons are given for a single unit of filter in Fig. 9(a) and also for the complete filter in Fig. 9(b). For the initial design, the resonators' coupling length is chosen to be 19.9 mm which is equal to $\lambda g/4$ at the center frequency of 2 GHz using RO4003c substrate. The input line width is also considered 0.2 mm which is equivalent to an impedance of 110 Ω. The spacing and

Table 2
Initial Dimensions of the Radials.

Notch Frequency (GHz)	3	6.4	9.8	13.2	16.6	20
Ro (mm)	10	5.7	4.2	5.2	4.6	4
θ (degree)	90	90	90	90	90	90
Wg (mm)	0.5	0.5	0.5	2	2	2

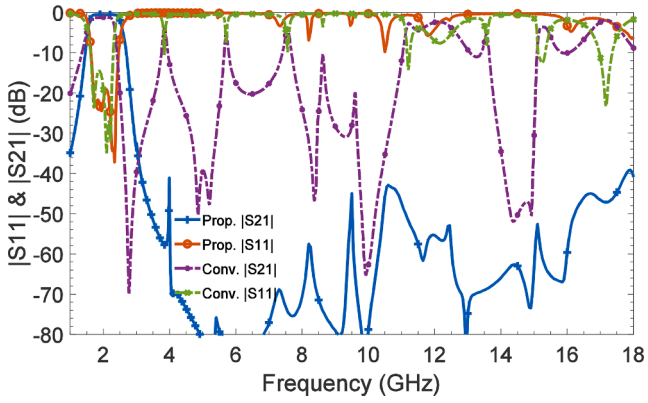

Fig. 10. Simulated frequency responses of the conventional hairpin filter and the proposed filter with embedded radial stubs.

width of the coupled lines are both 0.2 mm which is equal to a KZ_1 value of 331.6. The initial value for the length of transmission lines between two consecutive radial stubs is chosen to be 3 mm according to Fig. 7. The initial value of two input and output transmission lines before and after consecutive radial stubs is considered zero for simplicity. The unit cell is chosen to be the middle resonator of the complete filter. The unit cell radial stub notches are located at 4 GHz and 11.5 GHz similar to the middle resonator of the final filter. The final unit cell response is obtained after optimization of full-wave simulation in HFSS. As it is shown in Fig. 9(a) the passband of the initial design of the unit cell is formed clearly but the return loss is not as good as the final design. The S21 responses follow a similar pattern for a large portion of the stopband. The discrepancies are expected due to the limited accuracy of the initial design. For the complete filter, the radial stubs are considered in a way to provide a uniform distribution of their notches in the desired stopband from 4 GHz to 20 GHz. The corresponding dimensions are given in Table 2. As observed from Fig. 9(b), the initial design S21 rejection behavior satisfies our expected stopband. The filter passband is formed around the center frequency but the inband return loss and bandwidth are not satisfying which is because of the finite capability of the initial design.

For the purpose of comparison, a conventional hairpin filter of the same order and with the same central frequency is designed and optimized on the same substrate. The responses of the regular filter and the proposed filter are depicted in Fig. 10. As can be seen, the stopband of the regular filter is limited to its second harmonic which is located at 4 GHz, whereas the proposed filter provides a suppression better than 40

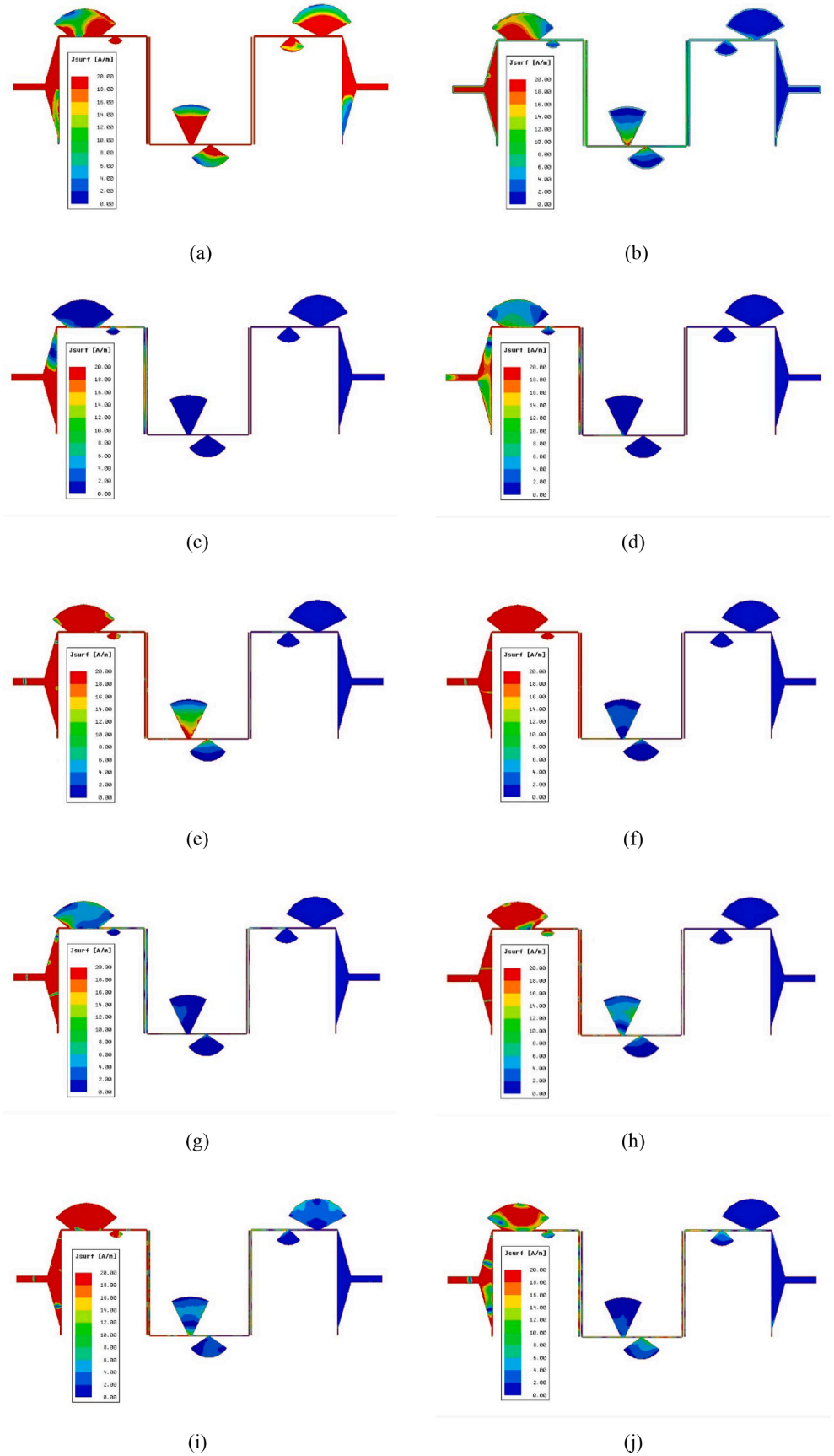

Fig. 11. Surface currents on filter structure at different frequencies after full-wave simulation in HFSS. (a) f = 2 GHz, (b) f = 4 GHz, (c) f = 6 GHz, (d) f = 8 GHz, (e) f = 10 GHz, (f) f = 12 GHz, (g) f = 14 GHz, (h) f = 16 GHz, (i) f = 18 GHz, (j) f = 20 GHz,

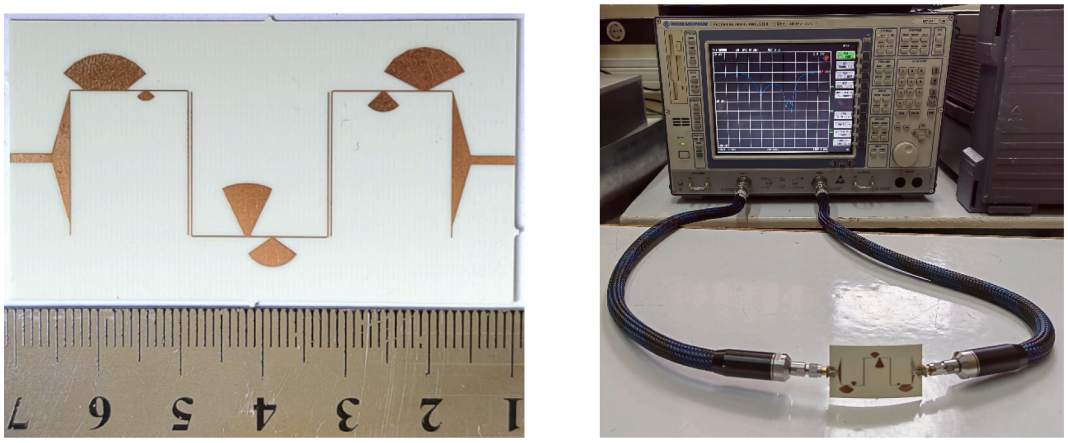

(a) (b)

Fig. 12. (a) Photograph of the fabricated 3rd-order filter, (b) Test setup.

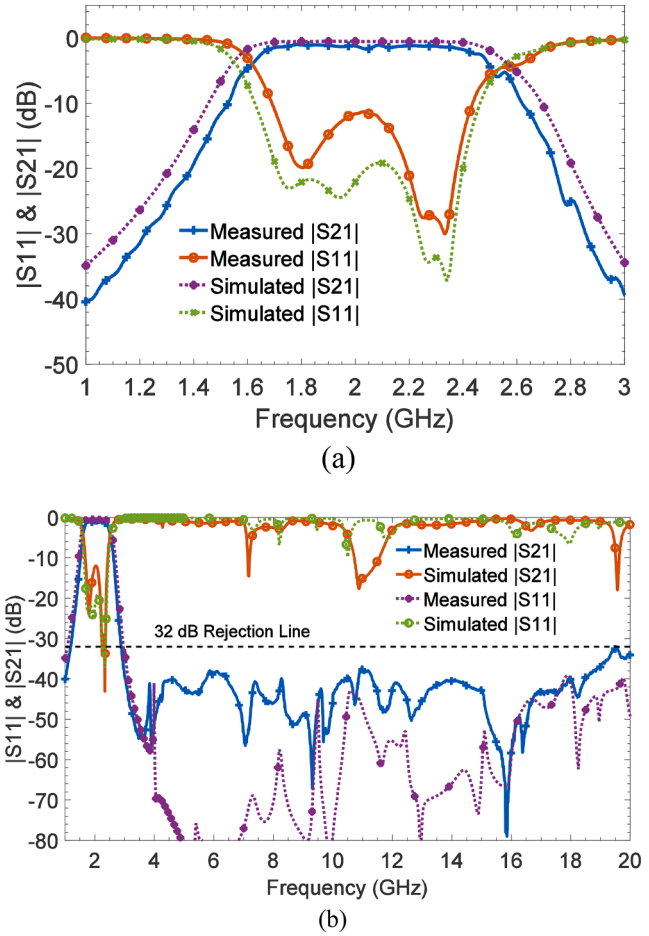

Fig. 13. Proposed filter simulated and experimental results. (a) Narrowband comparison. (b) Wideband comparison.

dB over a broad bandwidth up to 18 GHz. Furthermore, the surface currents on the filter structure are plotted for the passband frequency and its suppressed harmonics. These plots are shown in Fig. 11. As it is evident, the only frequency in which a strong current distribution can be observed is the center frequency of the passband which is shown in Fig. 11(a). All the other current distributions corresponding to harmonics up to 20 GHz that are shown in Fig. 11(b)-(j) have a very weak distribution compared to Fig. 11(a). These currents are extremely dampened by the presence of the radial stubs and therefore cannot pass through the filter and therefore the expected wide stopband is provided.

Fig. 12 displays the photograph of the fabricated filter and the measurement test setup. The measurement was performed using Rohde & Schwarz ZVK vector network analyzer. The ZV-Z34 calibration kit was used for the calibration procedure. The comparison between the measurement and simulation results of the proposed filter is illustrated in Fig. 13(a)-(b). As is clear from Fig. 13, there are good agreements between measured and simulated results in the passband and stopband. As expected, there is a shrinkage in the bandwidth of the passband which is shown in Fig. 13(a). The 3 dB bandwidth of the filter is from 1.6 GHz to 2.5 GHz which is equal to 44% and the insertion loss of the filter is 1.3 dB. The return loss in the passband follows an almost exact replica of the shape of the simulated response. The spurious suppression level of the proposed filter for frequency range of 3 GHz to 20 GHz is better than 32 dB. The discrepancies in the agreement of two series of results can be attributed to different factors such as the presence of solders, the quality of SMA connectors, and non-ideal characteristics in the fabricated RF board.

A comparison of the experimental results of the proposed filter and some other recent filters featuring wide stopbands is given in Table 3. These filters are chosen from the references based on the superiority of performance. In the column “Extra Features” of the table, any special requirement and complexity in fabrication process is mentioned. These features can especially decrease the reliability of the filters.

5. Conclusion

A new structure for a bandpass filter based on a hairpin structure with two embedded radial stubs in each resonator is presented. The proposed filter was implemented on RO4003c substrate and its performance was verified with experimental results and a wide stopband of $10f_0$ with good rejection level of 32 dB were observed. This filter can be easily implemented in off-the-shelf-ICs based RF modules, such as synthesizers implemented by frequency multipliers, where there are fewer constraints on size compared to some other applications areas such as MMICs.

The filter can also be simplified and reduced in size depending on its application, desired rejection bandwidth, and suppression level. These simplifications can be performed using only one embedded radial for each resonator, or even using single radial stubs for some resonators and not all of them. These changes will result in a relatively smaller stopband and rejection and also a smaller filter size. Even a modified small version of the filter can be considered for circuits such as frequency multiplier MMICs to filter out the undesired multiplication products and provide

Table 3
Comparison of the filter performances.

Ref.	Technique	Filter Order	IL	RL[a]	Size (λg)	Extra Features	HS	SL
[18]	Cross Coupling	–	2.2	−8	0.4 × 0.3	–	$3.3\,f_0$	30
[23]	Nonuniform Lines	3	N.A.	−19.6	1.1 × 0.3	–	$2\,f_0$	40
[24]	SIR Cells	3	2.5	−15	1.6 × 0.3	Multilayered	$3\,f_0$	30
[25][b]	Stepped Impedance	3	0.78	–22.1	1.2 × 0.4	–	$2\,f_0$	40
[26]	Grooved Substrate	3	2	−12.4	N.A.	Substrate Groove	$2\,f_0$	35
[29]	Wiggly Lines	7	2	−15	N.A.	–	$4\,f_0$	30
[30]	Shortened Lines	4	1.6	−9.9	N.A.	Via	$7.4\,f_0$	30
[31]	Stub Loading	–	1.2	−19	0.08 × 0.08	Via	$4.9\,f_0$	27.5
[32][c]	Stub Loading	3	2	−18	0.3 × 0.1	Via	$8.7\,f_0$	25
This work	Radial Stubs	3	1.3	−11.3	0.64 × 0.43	None	$10\,f_0$	32

IL = Insertion Loss (dB), RL = Return Loss (dB), HS = Harmonic Suppression, SL = Suppression Level (dB).
[a] The worst inband return loss is reported for the return loss.
[b] The filter with 25% bandwidth is considered.
[c] The PC-SLR bandpass filter with optimized nonsymmetrical U corners is considered.

an output with a cleaner spectrum. Finally, it is noteworthy to mention that using this filter in industries with mass production, such as the automotive radar industry, can be particularly beneficial. In these industries, there is a special emphasis on using elements with structures as simple as possible to increase robustness to different production tolerances for the large number of products. The proposed filter does not require any special structures such as DGS, multilayers, or even vias which can be considered as an important factor for these industries and anywhere there is a high demand for cost minimization and good performance at the same time. There is also ongoing work by the authors to achieve more suppression in the stopband and also design an enclosure that will not degrade the filter performance due to cavity modes.

Declaration of Competing Interest

The authors declare that they have no known competing financial interests or personal relationships that could have appeared to influence the work reported in this paper.

Data availability

No data was used for the research described in the article.

References

[1] Killamsetty VK, Mukherjee B. Compact triple band bandpass filters design using mixed coupled resonators. AEU-Int J Electron Commun 2019;107:49–56. https://doi.org/10.1016/j.aeue.2019.03.005.
[2] Mazar H. The radio frequency spectrum and wireless communications. In: Radio Spectrum Management: Policies, Regulations and Techniques. 1st ed. Chichester, UK: Wiley; 2016. p. 3–4. ch. 1, sec. 4,.
[3] Kazimierczuk MK, Introduction. In: RF Power Amplifiers. 1st ed. Chichester, UK: Wiley, 2008, ch. 1, sec. 13, pp. 23-25.
[4] Bera SC. Microwave communication systems. In: Microwave Active Devices and Circuits for Communication. 1st ed. Singapore: Springer Singapore, 2019, ch.19, sec. 3, pp. 593-598.
[5] Chang K. Various components and their system parameters. In: RF and Microwave Wireless Systems. 1st ed. New York, NY, USA: Wiley; 2000. p. 143–5. ch. 4, sec. 8,.
[6] Vizmuller P. Circuit examples. In: RF Design Guide: Systems, Circuits, and Equations. 1st ed. Boston, MA, USA: Artech House, 1995, ch. 2, sec. 11, pp. 123-125.
[7] Cameron RJ, Kudsia CM, Mansour RR. Microwave resonators. In: Microwave filters for communication systems: fundamentals, design and applications. 2nd ed. Hoboken, NJ, USA: Wiley, 2018, ch. 11, sec. 1, pp. 373-376.
[8] Jarry P, Beneat J. Microwave filter structures. In: Design and realizations of miniaturized fractal RF and microwave filters. 1st ed. Hoboken, NJ, USA: Wiley, 2009, ch. 1, sec. 3, p. 13.
[9] Abdel-Aziz M, Abd El-Hameed AS, Awamry AA, Mohra AS. Dual-band broadside-coupled based BPF with improved performance. AEU-Int J Electron Commun 2021; 138:153895. https://doi.org/10.1016/j.aeue.2021.153895.
[10] Cohn S. Direct-coupled-resonator filters. Proc IRE 1957;45(2):187–96. https://doi.org/10.1109/JRPROC.1957.278389.
[11] Cohn SB. Parallel-coupled transmission-line-resonator filters. IEEE Trans Microw Theory Techn 1958;6(2):223–31. https://doi.org/10.1109/TMTT.1958.1124542.
[12] Cristal EG, Frankel S. Hairpin-line and hybrid hairpin-line/half-wave parallel-coupled-line filters. IEEE Trans Microw Theory Techn 1972;20(11):719–28. https://doi.org/10.1109/TMTT.1972.1127860.
[13] Kuo J-T, Chen S-P, Jiang M. Parallel-coupled microstrip filters with over-coupled end stages for suppression of spurious responses. IEEE Microw Wirel Compon Lett 2003;13(10):440–2. https://doi.org/10.1109/LMWC.2003.818531.
[14] Velazquez-Ahumada M, Martel J, Medina F. Parallel coupled microstrip filters with ground-plane aperture for spurious band suppression and enhanced coupling. IEEE Trans Microw Theory Techn 2004;52(3):1082–6. https://doi.org/10.1109/TMTT.2004.823593.
[15] Kuo J-T, Jiang M, Chang H-J. Design of parallel-coupled microstrip filters with suppression of spurious resonances using substrate suspension. IEEE Trans Microw Theory Techn 2004;52(1):83–9. https://doi.org/10.1109/TMTT.2003.821247.
[16] Garcia-Garcia J, et al. Spurious passband suppression in microstrip coupled line band pass filters by means of split ring resonators. IEEE Microw Wirel Compon Lett 2004;14(9):416–8. https://doi.org/10.1109/LMWC.2004.832066.
[17] Wang S-M, Chi C-H, Hsieh M-Y, Chang C-Y. Miniaturized spurious passband suppression microstrip filter using meandered parallel coupled lines. IEEE Trans Microw Theory Techn 2005;53(2):747–53. https://doi.org/10.1109/TMTT.2004.840619.
[18] Chang KF, Tam KW. Miniaturized cross-coupled filter with second and third spurious responses suppression. IEEE Microw Wirel Compon Lett 2005;15(2): 122–4. https://doi.org/10.1109/LMWC.2004.842857.
[19] Ghalibafan J, Fallahzadeh S, Komjani N, Tayarani M. Design of a compact hairpin filter with spurious suppression. J Electromagn Waves Appl 2011;25(7):1059–67. https://doi.org/10.1163/156939311795253966.
[20] Lotfi-Neyestanak AA, Lalbakhsh A. Improved microstrip hairpin-line bandpass filters for spurious response suppression. Electron Lett 2012;48(14):858–9. https://doi.org/10.1049/el.2012.0967.
[21] Kim IK, et al. Fractal-shaped microstrip coupled-line bandpass filters for suppression of second harmonic. IEEE Trans Microw Theory Techn 2005;53(9): 2943–8. https://doi.org/10.1109/TMTT.2005.854263.
[22] Chen W-L, Wang G-M. Effective design of novel compact fractal-shaped microstrip coupled-line bandpass filters for suppression of the second harmonic. IEEE Microw Wirel Compon Lett 2009;19(2):74–6. https://doi.org/10.1109/LMWC.2008.2011311.
[23] Sun S, Zhu L. Periodically nonuniform coupled microstrip-line filters with harmonic suppression using transmission zero reallocation. IEEE Trans Microw Theory Techn 2005;53(5):1817–22. https://doi.org/10.1109/TMTT.2005.847079.
[24] Kuan H, Lin Y-L, Yang R-Y, Chang Y-C. A multilayered parallel coupled microstrip bandpass filter with embedded SIR cells to have a broad upper rejection band. IEEE Microw Wirel Compon Lett 2010;20(1):25–7. https://doi.org/10.1109/LMWC.2009.2035957.

[25] Worapishet A, Srisathit K, Surakampontorn W. Stepped-impedance coupled resonators for implementation of parallel coupled microstrip filters with spurious band suppression. IEEE Trans Microw Theory Techn 2012;60(6):1540–8. https://doi.org/10.1109/TMTT.2012.2190743.
[26] Moradian M, Tayarani M. Spurious-response suppression in microstrip parallel-coupled bandpass filters by grooved substrates. IEEE Trans Microw Theory Techn 2008;56(7):1707–13. https://doi.org/10.1109/TMTT.2008.925239.
[27] Das TK, Chatterjee S. Harmonic suppression by using T-shaped spur-Line in a compact hairpin-line bandpass filter. Radioengineering 2021;30(2):296–303. https://doi.org/10.13164/re.2021.0296.
[28] Das TK, Chakraborty A, Chatterjee S, Gupta B. Centrally corrugated cross-coupled wide stopband folded bandpass filter with spurline. In: 2022 Microw. Mediterranean Symp. (MMS), Pizzo Calabro, Italy, May 2022, pp. 1–6. doi: 10.1109/MMS55062.2022.9825567.
[29] Lopetegi T, et al. Microstrip 'wiggly-line' bandpass filters with multispurious rejection. IEEE Microw Wirel Compon Lett 2004;14(11):531–3. https://doi.org/10.1109/LMWC.2004.837062.
[30] Chao-Huang Wu, Lin Y-S, Wang C-H, Chen CH. Novel microstrip coupled-line bandpass filters with shortened coupled sections for stopband extension. IEEE Trans Microw Theory Techn 2006;54(2):540–6. https://doi.org/10.1109/TMTT.2005.862710.
[31] Killamsetty VK, Mukherjee B. Compact selective bandpass filter with wide stopband for TETRA band applications. IEEE Trans Compon Packag Manuf Technol 2018;8(4):653–9. https://doi.org/10.1109/TCPMT.2018.2803218.
[32] Akra M, Pistono E, Issa H, Jrad A, Ferrari P. Full study of the parallel-coupled stub-loaded resonator: synthesis method in a narrow band with an extended optimal rejection bandwidth. IEEE Trans Microw Theory Techn 2014;62(12):3380–92. https://doi.org/10.1109/TMTT.2014.2364599.
[33] Vryonides P, Arain S, Quddious A, Antoniades MA, Nikolaou S. A novel S-band bandpass filter (BPF) with extremely broad stopband. In: 2018 48th Eur. Microw. Conf. (EuMC), Madrid, Spain, Sep. 2018, pp. 954–957. doi: 10.23919/EuMC.2018.8541570.
[34] Lu S, Xu K-D, Liu Y, Guo Y-J. Bandpass filters using stepped coupled lines with super wide stopbands. IEEE J Radio Freq Identif 2022;6:97–103. https://doi.org/10.1109/JRFID.2021.3120376.
[35] Pozar DM. Microwave filters. In: Microwave engineering. 4th ed. Hoboken, NJ, USA: Wiley; 2012. p. 426–35. ch. 8, sec. 7.
[36] Pozar DM. Microwave network analysis. In: Microwave engineering. 4th ed. Hoboken, NJ, USA: Wiley, 2012, ch. 4, sec. 4, p. 190.
[37] March SL. Analyzing Lossy Radial-Line Stubs (Short Papers). IEEE Trans Microw Theory Techn 1985;33(3):269–71. https://doi.org/10.1109/TMTT.1985.1132997.